3-13-2003

Stability of Order in Solvent-Annealed Block Copolymer Thin Films

Sanjun Niu
University of Nenraska-Lincoln, sniu2@unl.edu

Ravi F. Saraf
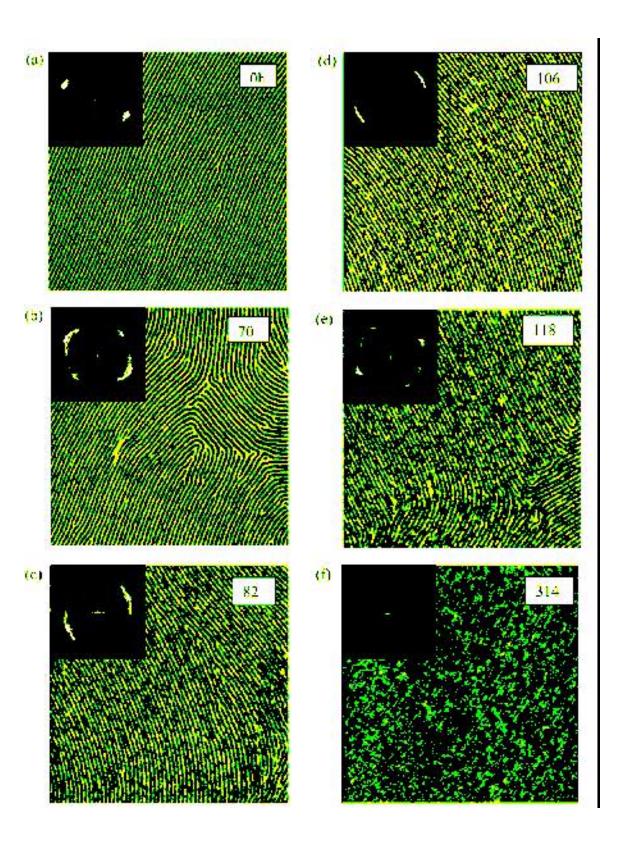*University of Nebraska-Lincoln*, rsaraf2@unl.edu

Stability of Order in Solvent-Annealed Block Copolymer Thin Films

Sanjun Niu and Ravi F. Saraf

ABSTRACT:

One way to produce high order in a block copolymer thin film is by solution casting a thin film and slowly evaporating the solvent in a sealed vessel. Such a solvent-annealing process is a versatile method to produce a highly ordered thin film of a block copolymer. However, the ordered structure of the film degrades over time when stored under ambient conditions. Remarkably, this aging process occurs in mesoscale thin films of polystyrene-polyisoprene triblock copolymer where the monolayer of vitrified 15 nm diameter polystyrene cylinders sink in a 20 nm thick film at 22 °C. The transformation is studied by atomic force microscopy (AFM). We describe the phenomena, characterize the aging process, and propose a semiquantitative model to explain the observations. The residual solvent effects are important but not the primary driving force for the aging process. The study may lead to effective avenue to improve order and make the morphology robust and possibly the solvent-annealing process more effective.

Figure 1. Typical 2 × 2 µm phase images of sample A obtained by AFM at the aging times indicated on each image. The inset of each image shows the corresponding fast Fourier transform (FFT). The lighter regions are PS cylinders. The sample is the same; however, the area imaged varies in each set.
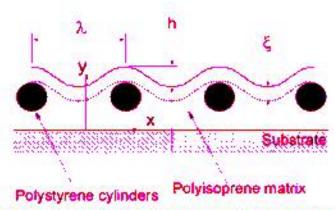
Figure 2. Schematic of the block copolymer monolayer with cylinders along the *z* axis and aligned parallel in the *x*-axis direction. Since PS has higher surface energy the air/film interface is PI. The period and amplitude of undulations due to the cylinders are λ and h. The "surface-layer" of thickness, ξ, is defined at the air/film interface with dotted line nominally tangent to the cylinder. This permeable PI membrane is conformal to part of PS cylinders.
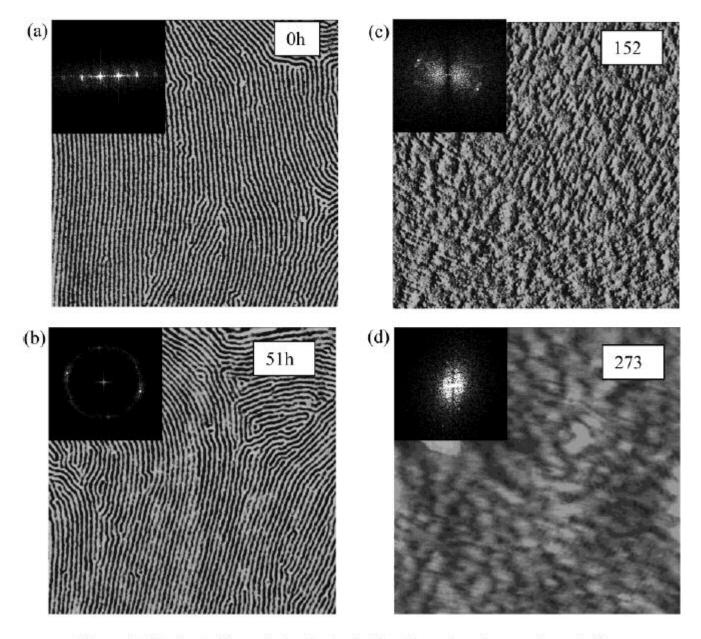
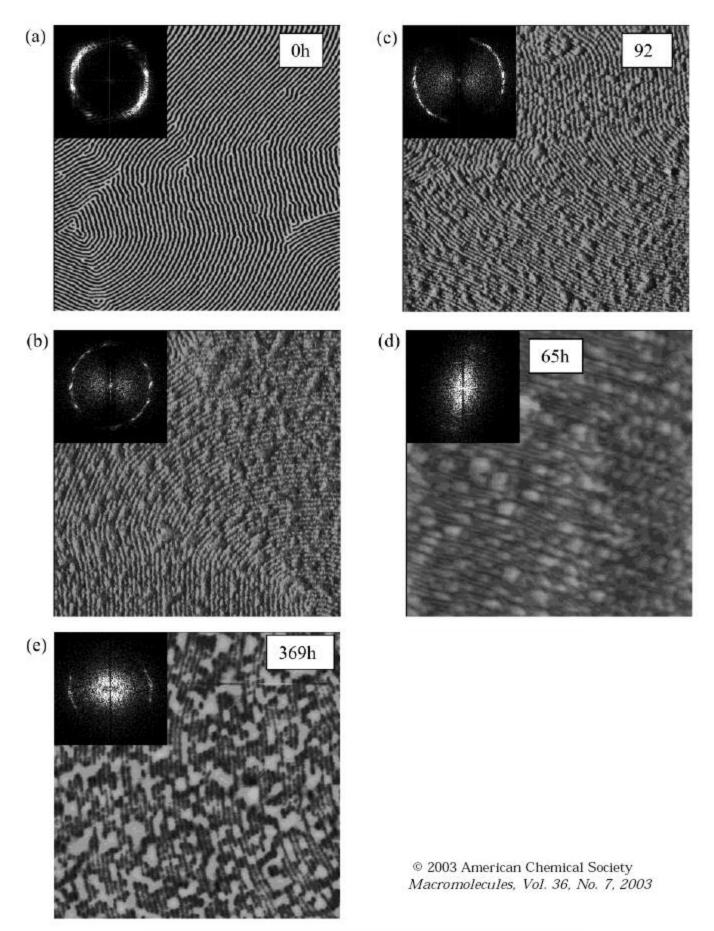**Figure 3.** Similar to Figure 1, showing typical 2 × 2 μm phase images of sample B.

(a) 0h
(b)
(c) 92
(d) 65h
(e) 369h

Figure 4. Similar to Figure 1, showing typical 2 × 2 μm phase images of sample C.
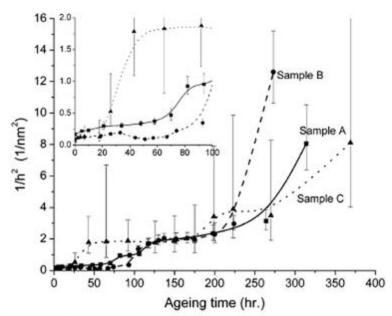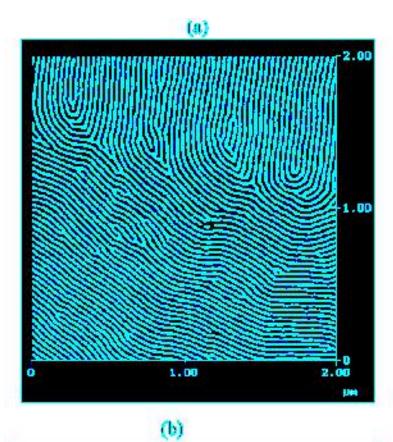
Figure 5. Changes in surface topography, $1/h^2$, compared as a function of aging time, t, for samples A, B, and C. The inset is a magnified view of the first 100 h of the aging behavior to indicate the complexities in sample B. The $h(0)$ for samples A, B, and C are 2.44 ± 0.413, 3.242 ± 0.0988, and 3.976 ± 0.132 nm, respectively.
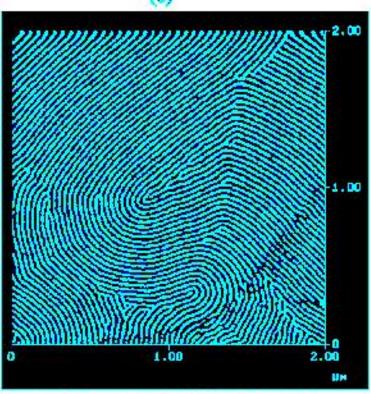
Figure 6. Comparison of typical 2 × 2 μm phase-images of sample A. (a) after solvent annealing (*t* = 0) and (b) (the same sample) after drying in 0.01 Torr vacuum at 60 °C for 3 h.
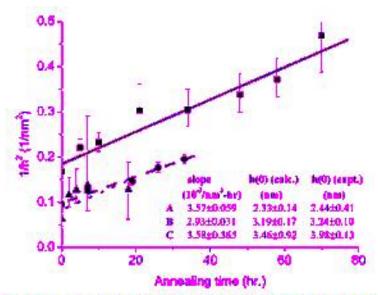
Figure 7. "Early-stage" aging behavior of samples A, B, and C. The data statistics is the same as in Figure 5. The straight line fit has R^2 of 0.957, 0.989, and 0.624, respectively. The values of $h(0)$ calculated from the intercept of the fitted line compares well with the measured value.
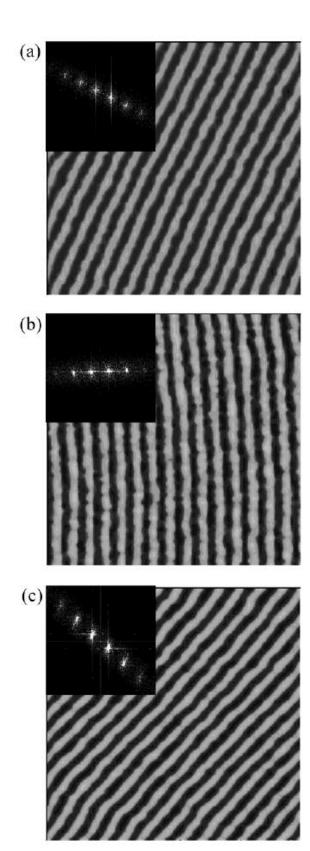
Figure 8. Typical $0.5 \times 0.5 \ \mu$m phase images at $t = 0$ h of (a) sample A, (b) sample B, and (c) sample C. The inset of each image shows the corresponding FFT. The lighter regions are PS cylinders.
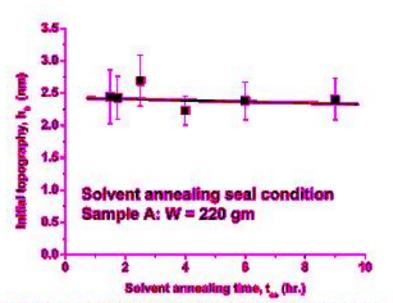
Figure 9. Initial height of various samples processed at $W =$ 220 g, similar to sample A, however the solvent-annealing time is varied from $t_{sa} = 1.5$ to 9 h. The statistics is identical to the Figure 5. Note that since the ordinate is h_0 rather than $1/h_0^2$, the error bars are symmetrical. The slope of the line -0.01027 ± 0.05219 is essentially zero, indicating that h_0 is constant for $t_{sa} > 1.5$ h at seal condition $W =$ 220 g. The average h_0 from the intercept is 2.42993 ± 0.26359 nm.
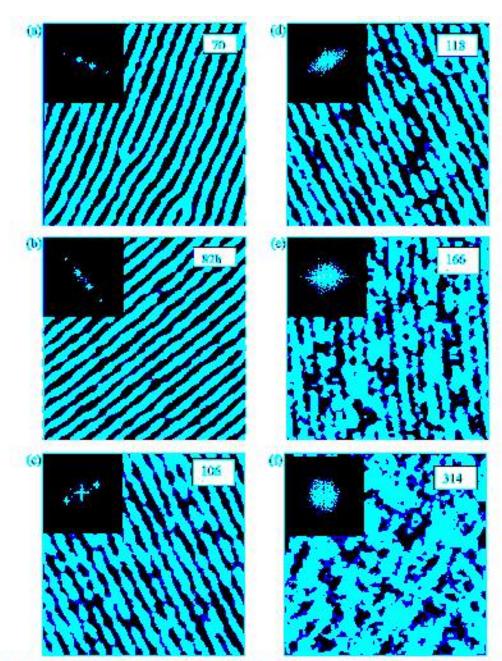
Figure 19. Typical 0.5 × 0.5 μm phase images of sample A obtained by AFM at the aging time indicated on each image. The inset of each image shows the corresponding fast Fourier transform (FFT). The lighter regions are PS cylinders. The sample is the same for the various images shown.
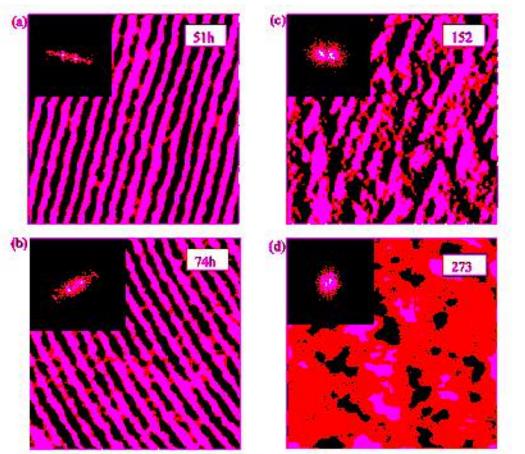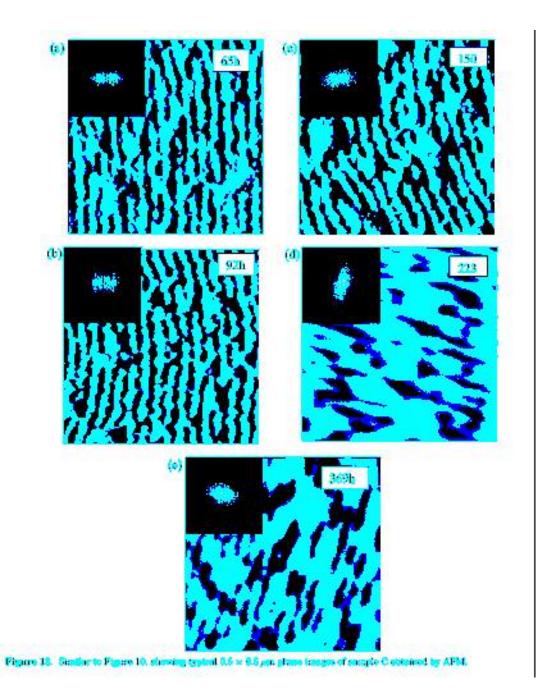
Figure 11. Similar to Figure 10, showing typical 0.5 × 0.5 μm phase images of sample B obtained by AFM.

Figure 12. Similar to Figure 10, showing typical 0.5 × 0.5 μm plane images of sample C obtained by AFM.
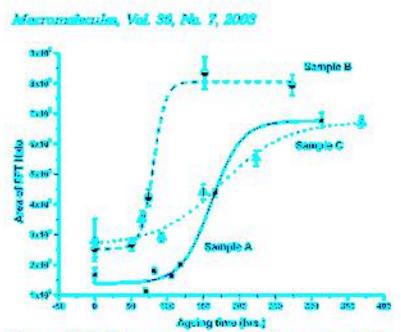
Figure 13. Total area under the central amorphous halo shown in Figures 10–12 as a function of aging time. To avoid any contribution from the structural signature of the cylinder packing (see insets of Figures 10–12), the slice is perpendicular to the axis of the cylinder. Furthermore, to avoid the FFT of the edges (for example in Figure 12b) images were analyzed with cylinders not parallel to the edges.